Proceedings of the 12th International Conference of Control Systems, and Robotics (CDSR 2025)
July 13, 2025 - July 15, 2025 | Imperial College London Conference Center, London, United Kingdom
Paper No. 107
DOI: 10.11159/cdsr25.107

Saturated Finite-Time High-Order Sliding Mode Control for Quadrotor-Based Search and Rescue with Deep Learning Person Detection

Aimen Abdelhak Messaoui[1, 2], Rabah Louali[2], Ali Zakaria Messaoui[2], Fethai Demim[2], Younes Samsar[3], Abdelkrim Nemra[2]
[1]Ecole Supérieure Ali Chabati
16036 Réghaia, Algeria
[2]Ecole Militaire Polytechnique
16046 Bordj El-Bahri, Algeria
[3]Université de Biskra, Algeria

Abstract **-** In search and rescue (SAR) operations, quadrotor UAVs play a critical role in the rapid and precise exploration of unknown areas. However, effective deployment requires robust control algorithms to handle environmental disturbances and high precision for mission-critical tasks. This paper presents a novel control algorithm, Saturated Finite-Time High-Order Sliding Mode Control, designed to enhance quadrotor performance under challenging conditions. The proposed algorithm is validated through a real-world SAR mission in which a quadrotor equipped with a camera utilizes SSD-Mobilenet-v2, a deep neural network-based object detection model, to locate a missing person. The SAR mission adopts a parallel grid search pattern for efficient area coverage. Experimental results demonstrate the control algorithm's robustness against vibrations and disturbances, enabling stable flight while maintaining accurate person detection from an altitude of 15 meters. The integration of advanced control and deep learning provides a reliable and effective solution for SAR missions. Future work will focus on improving detection accuracy through additional training and enhancing vibration mitigation.

Keywords**:** Quadrotor system, saturated/ Bounded control, Finite-time convergence, high-order sliding mode control, Search and rescue, SSD-Mobilenet-v2.

1. Introduction

In recent years, the use of aerial robots, particularly quadrotors, has gained significant attention in search and rescue (SAR) operations, particularly in hazardous or hard-to-reach areas like forests, mountains, or disaster-stricken zones [1]. In these environments, rapid response is crucial, as it can mean the difference between life and death. With their vertical takeoff and landing capabilities, exceptional maneuverability, and hovering ability, quadrotors are ideally suited for SAR tasks. They can quickly cover large areas, provide real-time situational awareness, and assist rescue teams in locating victims. This integration of robotics enhances operational efficiency and reduces the risks to human rescuers [2].

Despite these advantages, quadrotors face significant challenges due to their inherently nonlinear dynamics, strong coupling, and underactuation. These issues complicate stabilization and control, particularly in the presence of disturbances like load perturbations, parametric uncertainty, and wind gusts [3]. To ensure reliable deployment in these unpredictable environments, robust control systems are needed. Additionally, integrating advanced perception systems to locate missing persons accurately remains a challenge. Although UAV technology has advanced, current systems still struggle with limited robustness against disturbances, imprecise detection, and inefficient area exploration, which hinders broader adoption in real-world SAR operations, where reliability and precision are crucial [4].

Key components of successful trajectory tracking in SAR missions are disturbance rejection, convergence time, and control boundedness. Control boundedness is particularly critical in ensuring stable operation and preventing issues like rotor saturation or overheating during intense maneuvers. Research emphasizes the simultaneous need to address control boundedness, finite-time convergence, and disturbance rejection, highlighting the need for both theoretical and practical solutions.

To overcome these challenges, research has focused on advanced control strategies. Adaptive neural control, for instance, has been explored to enhance stability by dynamically adjusting parameters [5] [6]. However, this approach faces

issues like "explosion of complexity" and limited feasibility for onboard implementation, along with a lack of stability proofs, raising concerns about its practical reliability.in addition to [7] the works [8] [9] also use traditional sliding mode-based techniques for stabilization, trajectory tracking, and robustness. Yet, its susceptibility to chattering effects can degrade performance, potentially damage motors, and induce vibrations that negatively affect detection accuracy. Furthermore, the use of linear sliding surfaces in SMC can limit convergence, making it inadequate for fast-response situations like SAR missions.

Finite-time control strategies, such as Non-Singular Fast Terminal Sliding Mode Control (FTSMC), have been explored to improve tracking performance under disturbances. For instance, the work in [10] emphasizes the enhancement of finite-time convergence to achieve better tracking performance. However, it does not address critical issues like actuator saturation, which is vital for maintaining stability during aggressive maneuvers. Similarly, the study in [11] investigates advanced finite-time techniques but also overlooks key aspects of actuator constraints, leaving room for improvement in practical implementation.

Bounded control strategies have also been proposed to handle input saturation and disturbances. The approach in [12] employs state transformations to manage input constraints effectively, focusing on ensuring bounded control signals. However, it heavily relies on accurate parameter identification, which can be challenging in scenarios with equipment limitations and inherent model uncertainties. Likewise, the work in [13] introduces adaptive frameworks to tackle uncertainties and disturbances, but its dependence on precise system modeling makes its application in real-world settings less feasible.

Although these strategies have improved quadrotor control, significant gaps remain. Few studies comprehensively address system uncertainties, actuator constraints, and external disturbances, and many lack experimental validation. Moreover, balancing disturbance rejection, finite-time convergence, and control boundedness in a single control framework remains a challenge.

This work addresses these gaps by proposing a novel Saturated Finite-Time High-Order Sliding Mode Control algorithm. This approach ensures stability, responsiveness, and disturbance rejection under demanding conditions. It is validated through a SAR mission, where a quadrotor equipped with a camera and leveraging the SSD-Mobilenet-v2 deep learning model detects and locates a missing person in a complex environment. By integrating robust control with advanced perception, this work takes a significant step toward realizing fully autonomous and efficient aerial SAR systems, offering a comprehensive solution to the challenges identified in the literature.

The key contributions of this study are highlighted by the following theoretical and practical aspects:

- Introducing a novel saturated homogeneous integral-type sliding manifold and designing a Saturated Finite-Time High-Order Sliding Mode Controller (SFTHOSMC) that ensures robustness against perturbations, bounded control signals, finite-time convergence of tracking errors, and eliminates chattering.
- Highlighting experimental results that validate the robustness of the proposed system against disturbances and its integration with advanced computer vision.
- Implementing a real-world SAR mission to validate the proposed control algorithm, combining it with the SSD-Mobilenet-v2 deep neural network for person detection.

The rest of the manuscript is organized as: Section 2 presents mathematical preliminaries. Section 3 presents the control design. Section 4 depicts experimental results and discussions. Finally, the conclusion and possible future works are discussed in Section 5.

2. Preliminaries and Problem Statement

2.1. Preliminaries

Consider the following dynamic system described by the differential equation

$$\dot{\mathrm{x}}(t) = f(t, \mathrm{x}), \qquad \mathrm{x}(0) = \mathrm{x}_0. \tag{1}$$

where x is the state vector, and $f(t, \mathrm{x})$: $\mathbb{R}_+ \times \mathbb{R}^n \to \mathbb{R}$ is a known nonlinear continuous function. In case where $f(t, \mathrm{x})$ is discontinuous, solutions of (1) are interpreted in Filippov sense [14].

Definition 1. [15]. The system (1) is globally finite-time stable if it is Global Asymptotic Stable and for any positive real number R, the system's trajectory starting within the disk $\|x\| < R$ converges to the origin and remain there after Finite-Time $T(x_0)$.

Definition 2. [16]. The system $\dot{\chi}_1(t) = \chi_2(t),\ \dot{\chi}_2(t) = -\lambda_1 sat_{\epsilon_1}\lceil\chi_1\rfloor^{\alpha_1} - \lambda_2 sat_{\epsilon_1}\lceil\chi_2\rfloor^{\alpha_2}$ with $\chi_i \in \mathbb{R}, (i = 1, 2)$ homogeneous in terms of dilation mapping $\Lambda_\lambda^\chi = \left[\lambda^{\frac{2-\alpha}{1-\alpha}}\chi_1,\ \lambda^{\frac{3-2\alpha}{1-\alpha}}\chi_2\right]^T$ for any $\lambda > 0$ with homogeneous degree $k = -1$ if the parameters are chosen by $\lambda_1, \lambda_2 > 0$ and $0 < \alpha < 1$.

.

2.2. Dynamic Model of the Quadrotor

A quadrotor is depicted within an earth-fixed frame (E-frame) and a body-fixed frame (B-frame), as shown in Fig 1. Using the Newton-Euler formalism in both the body and inertial frames, the equations governing positional motion can be derived as follows [17]

$$\begin{cases} \ddot{x} = -m^{-1}[(c\phi s\theta c\psi - s\phi s\psi)u_z - k_x\dot{x} + d_x^{\text{ext}}], \\ \ddot{y} = -m^{-1}\left[(c\phi s\theta c\psi - s\phi s\psi)u_z - k_y\dot{y} + d_y^{\text{ext}}\right], \\ \ddot{z} = -m^{-1}[(c\phi c\theta)u_z - k_z\dot{z} + d_z^{\text{ext}}] + g. \end{cases} \tag{2}$$

The position of the aircraft's center of mass is denoted by $x, y, z \in \mathbb{R}^3$, $\dot{x}, \dot{y}, \dot{z} \in \mathbb{R}^3$ and $\ddot{x}, \ddot{y}, \ddot{z} \in \mathbb{R}^3$ represent the first- and second-time derivatives of the position variables, respectively. $\mathrm{K}_x, \mathrm{K}_y, \mathrm{K}_z \in \mathbb{R}_+$, g denotes gravitational acceleration, The thrust force created by the four rotors is represented by u_z and the exogenous perturbations are represented as $d_x^{\text{ext}}, d_y^{\text{ext}}, d_z^{\text{ext}}$. additionally, the trigonometric functions cosine and sine are abbreviated as $c()$ and $s()$ correspondingly

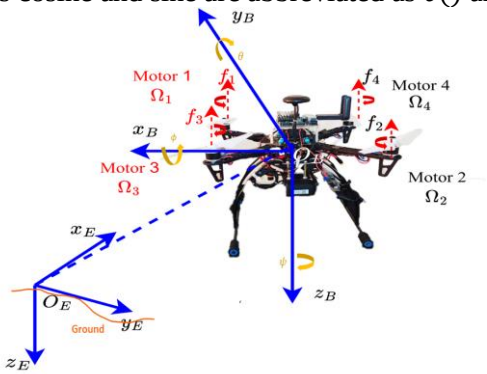

Fig 1. quadrotor representation in both B-frame and E-frame.

The mathematical model of the quadrotor's position can be rewritten in state-space representation to facilitate the development of an appropriate control design as follows

$$\begin{cases} \dot{x}_1 = x_2, \\ \dot{x}_2 = -\mathcal{P}_5^{\mathcal{N}}(cx_1sx_3cx_5 + sx_1sx_5)u_z + d_x^{\text{lum}}, \\ \dot{x}_3 = x_4, \\ \dot{x}_4 = -\mathcal{P}_5^{\mathcal{N}}(cx_1sx_3cx_5 + sx_1sx_5)u_z + d_y^{\text{lum}}, \\ \dot{x}_5 = x_6, \\ \dot{x}_6 = -\mathcal{P}_5^{\mathcal{N}}(cx_1cx_3)u_z + \mathrm{g} + d_z^{\text{lum}}. \end{cases} \tag{3}$$

where $x \stackrel{\text{def}}{=} [x \quad \dot{x} \quad y \quad \dot{y} \quad z \quad \dot{z}] \in \mathbb{R}^6$ is the state vector.

The system in equation (3) is a nonlinear, underactuated, multi-input, multi-output system, subject to perturbations, making flight control design challenging. A perturbed second-order system is derived for control design

$$\begin{cases}\dot{\chi}_1(t) = \chi_2(t), \\ \dot{\chi}_2(t) = F_\xi\left(\chi_1, \mathcal{P}_5^{\mathcal{N}}, t\right) + d_\xi^{\text{lum}}\left(d_\xi^{\text{ext}}, d_\xi^{\text{unm}}, t\right), \\ \mathcal{Y}_1(t) = \chi_1(t). \end{cases} \tag{4}$$

where $X_\xi \triangleq [\chi_1 \quad \chi_2]^T \in \mathbb{R}^{3\times 2}$ is the vector of states, $\chi_1 \triangleq \xi = [x_1 \quad x_3 \quad x_5]^T = [x \quad y \quad z]^T$, $\chi_2 \triangleq \dot{\xi} = \mathcal{V} = [x_2 \quad x_4 \quad x_6]^T = [\dot{x} \quad \dot{y} \quad \dot{z}]^T = [v_x \quad v_y \quad v_z]^T$ and $\mathcal{Y}_1 \triangleq [x \quad y \quad z]^T \in \mathbb{R}^3$ is the outputs, and $d_\xi^{\text{lum}} \triangleq \left[d_\phi^{\text{lum}} \quad d_\theta^{\text{lum}} \quad d_\psi^{\text{lum}}\right]^T \in \mathbb{R}^3$ is the lumped disturbances. The definition of the physical entity $F_\xi \neq 0$ that represents the position system's virtual control inputs is...

$$F_\xi \triangleq \begin{bmatrix} F_x \\ F_y \\ F_z \end{bmatrix} = \begin{bmatrix} -u_z(m)^{-1}(c\phi s\theta c\psi - s\phi s\psi) \\ -u_z(m)^{-1}(c\phi s\theta c\psi - s\phi s\psi) \\ -u_z(m)^{-1}(c\phi c\theta) + g \end{bmatrix}. \tag{5}$$

Definition 3. (Control problem) This study aims to design a bounded robust flight controller for a nonlinear, disturbed quadrotor, tailored for search and rescue (SAR) missions. The control performance requirements are:

- Bounded control signals within physical limits.
- Effective disturbance rejection to handle challenging environmental factors in SAR scenarios.
- Smooth, singularity-free, and chattering-free control.

Stability of the global feedback-loop system.

3. Main Results

3.1. Control Design

Let us define the position tracking errors and its dynamics as

$$\begin{cases} e_1^\xi = \xi - \xi_d \\ e_2^\xi = \dot{\xi}_d - \dot{\xi}_d \end{cases} \tag{6}$$

after differentiating (6) we get

$$\begin{cases} \dot{e}_1^\xi = e_2^\xi \\ \dot{e}_2^\xi = \ddot{\xi} - \ddot{\xi}_d \end{cases} \tag{7}$$

the novel sliding surface is introduced as

$$s_\xi \triangleq e_2^\xi + \int \lambda_1^\xi \text{sat}_{\epsilon_1}\left[e_1^\xi\right]^{\alpha_1} + \lambda_2^\xi \text{sat}_{\epsilon_1}\left[e_2^\xi\right]^{\alpha_2} dt \tag{8}$$

where $\lambda_1^\xi, \lambda_1^\xi \in \mathbb{R}^+$ are the control gains and $\alpha_1 = \frac{\alpha}{2-\alpha}$ and $\alpha_2 = \alpha$ with $\alpha \in (0,1)$. Consequently, we propose the following composite tracking controller to establish both phases of the SMC, i.e., reaching phase and sliding phase

$$u_\xi \triangleq u_r^\xi + u_{eq}^\xi \tag{9}$$

the equivalent control term u_{eq}^{ξ} maintains the system states on $s_{\xi} = 0$ within finite time while mitigating disturbances. Meanwhile, the reaching control term u_r^{ξ} ensures finite-time convergence to the sliding manifold $s_{\Theta} = 0$.

The reaching law u_r^{Θ} is proposed as

$$u_r^{\xi} \triangleq k_1^{\xi} \mathrm{sat}_{\epsilon_2} \lceil s_{\xi} \rfloor^{\frac{1}{2}} + w_{\xi} \tag{10}$$

$$\dot{w}_{\xi} \triangleq -k_2^{\xi} \mathrm{sgn}(s_{\xi}) - k_3^{\xi} w_{\xi} \tag{11}$$

with $k_1^{\xi}, k_3^{\xi} \in \mathbb{R}^+$ and $k_2^{\xi} > 2L_{\xi} + \frac{9L_{\xi}^2}{4k_1^{\xi^2}}$, with $L_{\xi} \triangleq k_3^{\xi} L_{\mathrm{M}}^{\xi} + L_m^{\xi}$ and the parameter ϵ_2 is chosen as $\epsilon_2 > \max\left\{ \frac{k_1^{\xi^2} + 2L_{\xi}}{2k_1^{\xi} k_3^{\xi}}, \frac{\left(k_1^{\xi^2} + 3L_{\xi}\right)^2 + 2L_{\xi} k_1^{\xi^2} + 2k_1^{\xi^2} k_2^{\xi}}{2k_1^{\xi} k_2^{\xi} k_3^{\xi}} \right\}$ [18].

The equivalent control is designed directly from the sliding surface dynamics $\dot{s}_{\xi} = 0$ (sliding manifold). Hence, from (8) The dynamics of the sliding manifold is given as

$$\dot{s}_{\xi} = \dot{e}_2^{\xi} + \lambda_1^{\xi} \mathrm{sat}_{\epsilon_1} \left[e_1^{\xi} \right]^{\alpha_1} + \lambda_2^{\xi} \mathrm{sat}_{\epsilon_1} \left[e_2^{\xi} \right]^{\alpha_2} \tag{12}$$

where the saturation parameter $\epsilon_1 \in \mathbb{R}^+$. We get from (4) and (7)

$$\dot{e}_2^{\xi} = F_{\xi} + d_{\xi}^{\mathrm{lum}} - \ddot{\xi}_d \tag{13}$$

Replacing $\dot{e}_2^{\xi}$ by its expression from (13) into (12) while considering $u_r^{\Theta} = 0$ and $u_{\xi} \equiv u_{eq}^{\xi}$, yields

$$u_{eq}^{\xi} \triangleq -\lambda_1^{\xi} \mathrm{sat}_{\epsilon_1} \left[e_1^{\xi} \right]^{\alpha_1} - \lambda_2^{\xi} \mathrm{sat}_{\epsilon_1} \left[e_2^{\xi} \right]^{\alpha_2} + \ddot{\xi}_d - d_{\xi}^{\mathrm{lum}} \tag{14}$$

the desired virtual controls are written as

$$F_{\xi}^{d} \triangleq -\lambda_1^{\xi} \mathrm{sat}_{\epsilon_1} \left[e_1^{\xi} \right]^{\alpha_1} - \lambda_2^{\xi} \mathrm{sat}_{\epsilon_1} \left[e_2^{\xi} \right]^{\alpha_2} + \ddot{\xi}_d - k_1^{\xi} \mathrm{sat}_{\epsilon_2} \lceil s_{\xi} \rfloor^{\frac{1}{2}} + w_{\xi} - d_{\xi}^{\mathrm{lum}} \tag{15}$$

where w_{ξ} is given by

$$\dot{w}_{\xi} \triangleq -k_2^{\xi} \mathrm{sgn}(s_{\xi}) - k_3^{\xi} w_{\xi} \tag{16}$$

the lift control u_z, along with the desired pitch ϕ_d and roll θ_d, are determined as

$u_z \triangleq m\sqrt{\left(F_x^d\right)^2 + \left(F_y^d\right)^2 + \left(F_z^d - g\right)^2}$,

$\phi_d \triangleq \arcsin\left[-\frac{m}{u_z} \left(F_x^d s\psi_d - F_y^d c\psi_d \right) \right]$ and

$\theta_d \triangleq \arcsin\left[-\frac{1}{F_z^d - g} \left(F_x^d c\psi_d - F_y^d s\psi_d \right) \right]$.

3.2. Stability Proof

Theorem 1. consider the synthesized nonlinear sliding surface s_{ξ}. Let the the system (4), characterized by second-order ODEs, be subjected to the saturated control input designed in (9) based on s_{ξ}. Consequently: **(i)** The tracking error e_1^{ξ} is

guaranteed to converge to the zero equilibrium in finite-time. **(ii)** The control input remains bounded over time. **(iii)** The upper bound on the control input is estimated by

$$\|u_\xi\|_\infty \leq (\lambda_1 + \lambda_2)\epsilon_1 + k_1\epsilon_1 + \frac{k_2}{k_3} + \overline{\ddot{\xi}_d}. \tag{17}$$

Additionally, w_ξ satisfies $\left|w_{\xi_i}(0)\right| \leq \frac{k_2}{k_3}$ with $w_{\xi_i}(0)$ being the ith element of $w_\Theta(0)$.

Proof. The proof is extensive and has been omitted here for brevity. However, it can be provided to interested readers upon request.

4. Experimental Results and Discussions

The proposed control algorithms for the quadrotor system are validated through real-time experiments in two phases. First, a 6-DOF outdoor flight experiment tests Cartesian trajectory tracking. The second phase involves a search and rescue (SAR) mission, where the quadrotor locates a person using a deep learning system. This two-stage experiment demonstrates the controller's feasibility and its practical application in a SAR operation. the position control parameters are chosen based on rigorous criteria as follows $\alpha = 0.78, \alpha_1 = \frac{\alpha}{2-\alpha} = 0.657, \alpha_2 = \alpha = 0.79, k_1^{\mathrm{x}} = k_1^{\mathrm{y}} = k_1^{\mathrm{z}} = 3.65, k_2^{\mathrm{x}} = k_2^{\mathrm{y}} = k_2^{\mathrm{z}} = 6.4,\ \epsilon_1 = 4,_1\ \lambda_1^{\mathrm{x}} = \lambda_1^{\mathrm{y}} = 7.5, \lambda_1^{\mathrm{z}} = 4, \lambda_2^{\mathrm{x}} = \lambda_2^{\mathrm{y}} = 3.2,\ \lambda_2^{\mathrm{z}} = 1.7, k_3^{\mathrm{x}} = k_3^{\mathrm{y}} = k_3^{\mathrm{z}} = 0.7, \epsilon_2 = 5.8.$

4.1. Outdoor Trajectory Tracking Validation

An outdoor flight experiment was conducted to validate the proposed controller. The quadrotor setup, shown in Fig 2, outlines the overall experimental configuration. The detailed hardware and software configuration layers used in the real outdoor flight experiment are illustrated in **Fig *3***. The system integrates a Pixhawk® autopilot running PX4 firmware 1.11.3, connected to an Nvidia Jetson Nano companion computer via UART. The Jetson Nano operates on Ubuntu Bionic 18.04, and a ROS environment with MAVROS manages real-time autopilot data. The control algorithm is implemented as a C++ ROS node, activated through a shell script.

(1) Radio telemetry module. (2) PC with QGround Control and Putty. (3) Radio Controller.
(4) WiFi Router. (5) GPS. (6) RC Receiver. (7) USB WiFi Adapter. (8) Pixhawk Autopilot.
(9) NVIDIA Jetson Nano. (10) LidarBenewake TF02-Pro.

Fig 2. The quadrotor aircraft's experimental setup for realistic outdoor flying.

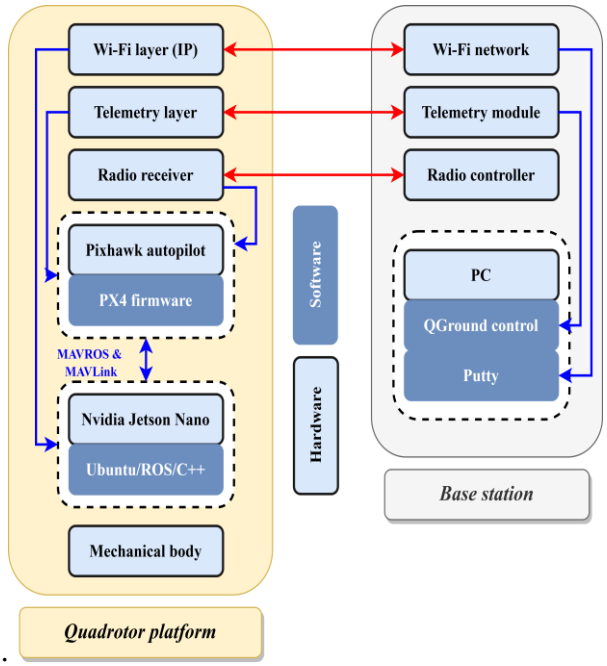

Fig 3. Configuration layers for the hardware and software in the actual outside flight experiment

A TP-LINK TL-AP1201P AC1200 Wi-Fi router establishes a local network, enabling remote access to the onboard computer via SSH. The ground station, equipped with an ASUS laptop (AMD Ryzen 7 3750H CPU, 16GB RAM, Windows 10 Pro), monitors flight data in real time using QGroundControl 4.2.4. The quadrotor's position (x, y) is tracked using an M8N GPS module, altitude (z) with a Benewake TF02-Pro lidar, and attitude variables (ϕ, θ, ψ) through the Pixhawk®'s Inertial Measurement Unit.

The practical realization of the proposed trajectory tracking controller, as illustrated in Fig 4, enables seamless operation through the integration of onboard computer and autopilot hardware. The trajectory tracking controller operates in Offboard Flight Mode, transmitting desired velocity commands (F_x^d, F_y^d, F_z^d). Its performance, benchmarked against a commercial PID controller, demonstrates precise 3-D and 2-D reference trajectory tracking, as depicted in Fig 5. Manual control remains possible via a radio controller, ensuring safety during operations.

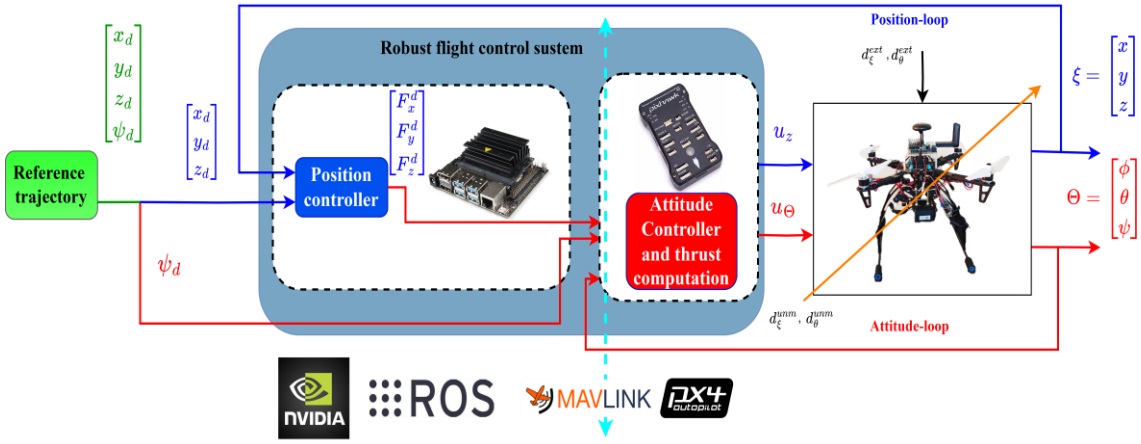

Fig 4. Diagram showcasing the implementation of the proposed trajectory tracking controller with onboard computer and autopilot integration.

Fig 6 and Fig 7 presenting the translational states and tracking errors for Cartesian positions. These figures demonstrate the proposed controller's ability to accurately maintain the quadrotor on the reference dynamic Cartesian trajectory, outperforming the pre-flashed PID controller. The calculated performance metrics, including the Integral of Squared Error (ISE), Root Mean Squared Error (RMSE), and Relative Dynamic Performance (RDP), are summarized in Table 1, highlighting significant reductions in tracking error. These improvements emphasize the effectiveness of the proposed controller compared to the PID control.

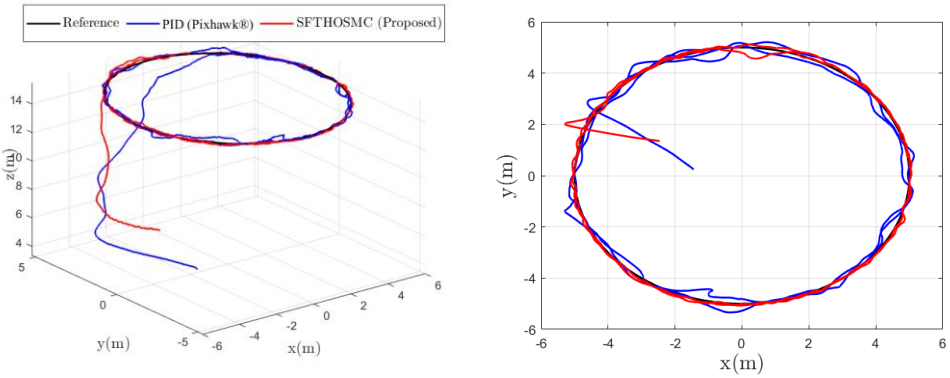

Fig 5. Evolution of the 3-D and 2-D trajectory tracking.

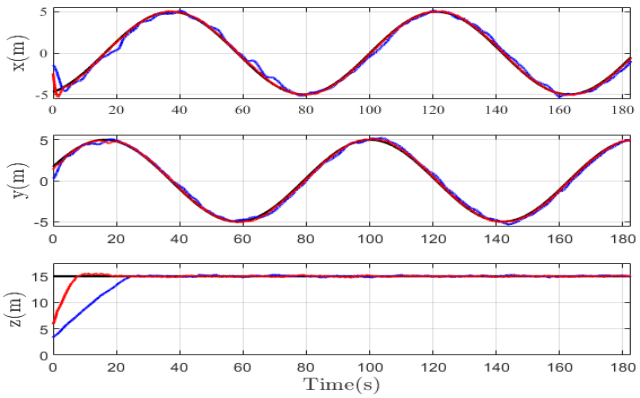

Fig 6. position states (x, y, z).Profiles

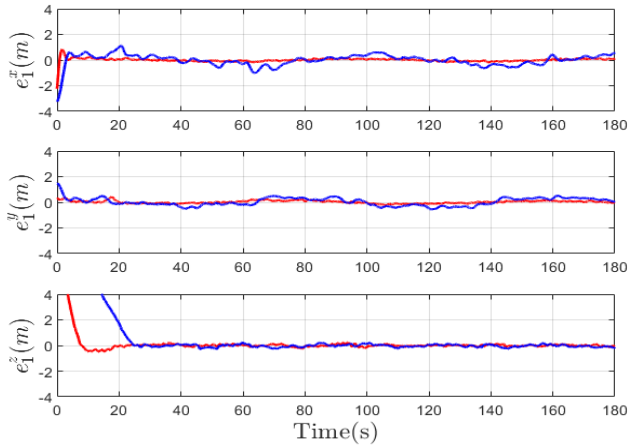

Fig 7. Position tracking errors (e_1^x, e_1^y, e_1^z).

Table 1. Evaluation of the RMSE and the ISE indexes by utilizing the RDP criterion (Experimental results).

Control strategy	Performance index					
	RMSE			ISE		
	e_1^x	e_1^y	e_1^z	e_1^x	e_1^y	e_1^z
PID (Pixhawk®)	0.447	0.307	2.332	7.242	3.427	1.979
SFTHOSMC (Proposed)	0.136	0.109	0.970	0.651	0.430	0.339
RDP (%)	**69.57**	**64.49**	**58.40**	**91.01**	**87.45**	**82.87**

4.1. Search and Rescue Mission

After completing the hardware design and validating the proposed controller through a 3D trajectory tracking test, this subsection presents a realistic search and rescue (SAR) mission to evaluate the performance of the proposed control algorithm. In our SAR scenario, we selected a parallel grid search pattern, as it has been shown to outperform the spiral grid design in terms of both effective area coverage and energy efficiency. A comparison study published in [19] supports this conclusion. Fig 8 illustrates an autonomous mission programmed with a parallel grid. During the mission, a missing individual is detected in an unknown area using a deep neural network (DNN) algorithm, specifically the MS COCO-pretrained SSD-Mobilenet-v2. This integration adds meaningful context to the search. The SSD-Mobilenet-v2 network, included in the Nvidia Jetson-inference package, is a computer vision-based deep learning system designed for object detection using pre-trained models. When used with the detectNet class, the algorithm processes input images and returns a list of bounding box coordinates, object classes, and confidence values.

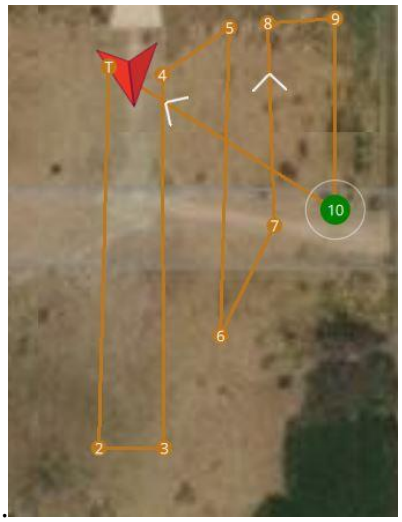

Fig 8. Search area scan using parallel grid-based flight planning.

Fig 9. Detection of lost persons in the search area using SSD-Mobilenet-v2 and detectNet classes.

As shown in Fig 9, the DNN algorithm successfully identifies the missing person while scanning the search region during flight. At an altitude of 15 meters, the algorithm achieves a detection accuracy of 86.6%. While similar industrial systems use gimbal-mounted cameras for vibration dampening (as vibrations can impair detection accuracy), our setup uses a camera fixed directly to the quadrotor's body. This configuration allows us to assess the chattering mitigation capabilities of the proposed flight control algorithm.

5. Conclusion

This research introduces a novel flight control algorithm for a quadrotor system, using an inner-outer loop framework and the SFTHOSMC approach to address under-actuation. The proposed controller ensures singularity elimination, fast convergence, and bounded, smooth control signals. The theoretical results are validated through experiments, demonstrating the controller's effectiveness in a real search and rescue scenario, where a pretrained SSD-Mobilenet-v2 and detectNet system locate a lost person.

Future work should extend this control to multi-quadrotor systems for larger area coverage, train the DNN model on new datasets for better accuracy, and explore Uniform Ultimate Boundedness (UUB) for closed-loop signals.

References

[1] A. A. Messaoui, S. Hakem, R. Louali, A. Amamra, A. Nemra and O. Mechali, "UAV-Based Search and Rescue System Using a Probability Distribution Map," in *International Conference on Networking and Advanced Systems (ICNAS)*, 2023.

[2] Y.Wang, W.Liu, J.Liu and C.Sun, "Cooperative USV–UAV marine search and rescue with visual navigation and reinforcement learning-based control," *ISA Transactions*, vol. 132, 2023.

[3] A. A. Messaoui, O. Mechali, A. Z. Messaoui, I. E. Smaali, "Robust Finite-Time Control of a Multirotor System via an Improved Optimized Homogeneous Twisting Control: Design and Validation," in *13th International Conference on Simulation and Modeling Methodologies, Technologies and Applications SIMULTECH*, Rome, Italy, 2023.

[4] I.Chekakta, K.Guelton, D.Jabri, D.E.Belkhiat and K.M.Motchon, "Regional T-S Model-based Attitude Tracking Control of a Quadrotor with Input Saturation and External Disturbances," *IFAC-PapersOnLine*, vol. 55, no. 15, pp. 63-68, 2022.

[5] P. Huang, J. Sun, X. Qin and J. Li, "A novel adaptive super-twisting trajectory tracking control with back propagation algorithm for a quadrotor UAV," *Proceedings of the Institution of Mechanical Engineers, Part I: Journal of Systems and Control Engineering*, 2024.

[6] A. Z. Messaoui, O. Mechali, A. A. Messaoui, I. E. Smaali, F. Demim and D. B. Djilali, “RBFNN-Based Optimized PID Control for a 3-DOF Helicopter System: Design and Validation,” in *8th International Conference on Image and Signal Processing and their Applications (ISPA)*, Biskra, Algeria, 2024.

[7] M. Herrera, W. Chamorro, A. P. Gómez and O. Camacho, “Sliding Mode Control: An Approach to Control a Quadrotor,” in *Asia-Pacific Conference on Computer Aided System Engineering*, Quito, Ecuador, 2015.

[8] D.J.Almakhles, “Robust Backstepping Sliding Mode Control for a Quadrotor Trajectory Tracking Application,” *IEEE Access,* vol. 8, pp. 5515-5525, 2020.

[9] Y. Wang, et al., “Quadrotor trajectory tracking and obstacle avoidance by chaotic grey wolf optimization-based backstepping control with sliding mode extended state observer,” *Trans. Inst. Meas. Control,* vol. 42, no. 9, pp. 1675-1689, 2020.

[10] A. Z. Messaoui, M. A. Alouane, M. Guiatni, O. Mechali, F. Sbargoud, Z. Serine and B. C. Elmokhtar, “Design and Control of Wearable Ankle Robotic Device,” in *ICINCO*, 2023.

[11] M. Labbadi, M. Cherkaoui, “Robust adaptive nonsingular fast terminal sliding-mode tracking control for an uncertain quadrotor UAV subjected to disturbances,” *ISA Transaction,* vol. 99, p. 290–304, 2020.

[12] C.Li, H.Zhao, H.Sun and Y.H.Chen, “Robust bounded control for nonlinear uncertain systems with inequality constraints,” *Mechanical Systems and Signal Processing,* vol. 140, p. 106665, 2020.

[13] H.Wang, G.Cui and H.Li, “Fixed-Time Adaptive Tracking Control for a Quadrotor Unmanned Aerial Vehicle with Input Saturation,” *Actuators,* vol. 12, 2023.

[14] A.F.Filippov, “Differential Equations with Discontinuous Righthand Sides,” in *Mathematics and Its Applications.*, 1988.

[15] A.Levant, “Homogeneity approach to high-order sliding mode design,” *Automatica,* vol. 41, no. 5, pp. 823-830, 2005.

[16] B.Tian, L.Yin and H.Wang, “Finite-Time Reentry Attitude Control Based on Adaptive Multivariable Disturbance Compensation,” *IEEE Transactions on Industrial Electronics,* vol. 62, no. 9, pp. 5889-5898, 2015.

[17] A. A. Messaoui, O. Mechali, R. Louali and A. Nemra , “Theory and experiment for autonomous quadrotor flight via bounded robust finite-time homogeneous sliding mode control: A roadmap to search and rescue,” *Proceedings of the Institution of Mechanical Engineers, Part I: Journal of Systems and Control Engineering,* 2024.

[18] B. Tian, Z. Li and Q. Zong, “A Continuous Multivariable Finite-Time Control Scheme for Double Integrator Systems With Bounded Control Input,” *IEEE Transactions on Automatic Control,* vol. 67, no. 11, pp. 6068-6073, Nov 2022.

[19] L.Xing, X.Fan, Y.Dong, Z.Xiong, L.Xing, Y.Yang, H.Bai, C.Zhou, “Multi-UAV cooperative system for search and rescue based on YOLOv5,” *International Journal of Disaster Risk Reduction,* vol. 76, p. 102972, 2022.